2020 IEEE 9th International Power Electronics and Motion Control Conference (IPEMC2020-ECCE Asia) | 978-1-7281-5301-8/20/$31.00 ©2020 IEEE | DOI: 10.1109/IPEMC-ECCEAsia48364.2020.9368128

Constant Power Load stabilization Based on Trajectory Control in Dual-Active-Bridge DC-DC Converter

Qinglei Bu, Huiqing Wen, Haochen Shi, Mingkai Zheng
Department of Electrical and Electronic Engineering
Xi'an Jiaotong-Liverpool University, 215123, Suzhou, China
E-mail: Qinglei.Bu@xjtlu.edu.cn; Huiqing.Wen@xjtlu.edu.cn

***Abstract*—This paper analysed the trajectory control (TC) based on natural switching surface (NSS) in dual-active-bridge (DAB) DC-DC converter. Which improves the fast transition process when load changes from constant resistor (CR) to constant power (CP). In order to obtain the NSS based state trajectory, the state-space equation is derived mathematically based on the small-signal model of DAB converter. Under the TC, the DAB can both achieve the constant power load (CPL) stability and fast start-up stage simultaneously . Finally, the comparison of open-loop control, closed-loop with linear controller and TC are given to validate the effectiveness of the proposed strategy.**

***Index Terms*—Bidirectional full bridge DC-DC converter, Constant power load, Transient-state, stabilization.**

I. Introduction

Because of the widely used distributed generating sources, DC microgrids are preferred as the interface of the power distribution system [1–4]. In DC microgrid system, due to the requirement of the bidirectional power conversion between various energy storage system, the bidirectional DC-DC converter plays a critical role [5–9]. It is usually placed between battery unit, ultracapacitor unit and DC buses as shown in Fig.1. Dual-active-bridge (DAB) DC-DC converter, which has the advantages of galvanic isolation, high voltage conversion ratio and zero-voltage-switching capability, is selected and depicted in Fig.2 [10–13]. In this converter, eight MOSFETs from S_1 to S_8 formed two full-bridges H1 and H2, which connected the high frequency transformer as the isolation. L represents the total inductance of leakage and auxiliary inductance.

As for the load terminal, constant resistive load and constant power load are frequently found in microgrid system. Compared with traditional CRL, the stability of the whole system is challenged because of the negative impedance instability of CPL [14–16]. To stabilize the CPL, passive stabilization methods were proposed by utilizing the RC and RL networks in converter [17]. However, these additional elements increase the complexity and reduce the transmission efficiency. One proposed methods named as circular switching surface technique based on buck+boost cascade converter is proposed to control the CPL [18]. However, the buck+boost converter cannot achieve the galvanic isolation and high voltage conversion ratio. NSS based boundary control was proposed for DAB in [19–23]. However, the load terminal is resistive load, the CPL condition is not mentioned. Thus, this paper analysed the trajectory control based on NSS for the DAB converter, especially to achieve the stability of CPL.

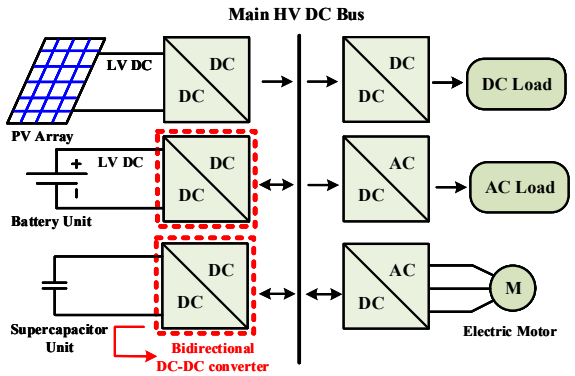

Fig. 1. Bidirectional DC-DC converter based microgrid

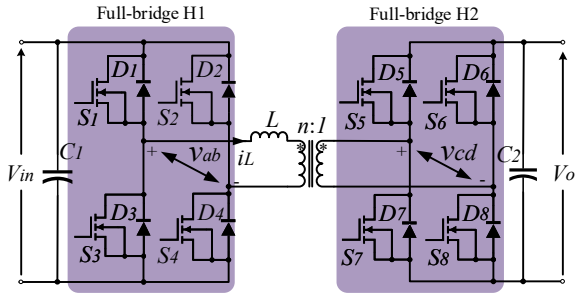

Fig. 2. Topology of dual-active-bridge DC-DC converter.

II. Constant Power Load and Proposed Improved Trajectory Control

A. Constant power load

Constant power load (CPL) are easily found in microgrid, which fed the power converters with the unique dynamic characteristics [14]. For example, the motor drive expressed the constant power (CP) behavior from the input terminal of DC bus under tight speed regulation. Another example is the DC-DC converter with tight voltage regulation. In CPLs, the multiplication of voltage and current is constant, which is shown in (1) and (2), although the instantaneous value of

impedance is positive, the derivative voltage with respect to current is negative shown in (3) and (4), which named as negative impedance instability and makes it difficult to control [14–16].

$$P_{CPL} = v \times i \tag{1}$$

$$R = \frac{v^2}{P_{CPL}} = \frac{P_{CPL}}{i^2} \tag{2}$$

$$\frac{\partial v}{\partial i} = -\frac{P_{CPL}}{i^2} \tag{3}$$

$$\frac{\partial R}{\partial i} = -\frac{2P_{CPL}}{i^3} \tag{4}$$

B. Natural switching surface based trajectory control

Natural switching surface (NSS) based trajectory can be derived from the inductor current i_L and the voltage of output capacitor u_{C2}. To simplify the control strategy, single-phase-shift control with four switching cases is adopted and shown in Fig.3. p_1 and p_2 stand for the parameter of bridge voltage v_{ab} and v_{cd}, which can also reflect the on off condition of each switches, $p_1 = 1$ stands for S_1 and S_4 on, $p_1 = -1$ stands for S_2 and S_3 on, $p_2 = 1$ stands for S_5 and S_8 on, $p_2 = -1$ stands for S_6 and S_7 on. Details are illustrated in Fig.3. The mathematical expression is shown in (5).

$$\begin{cases} v_{ab} = p_1 V_{in} \\ v_{cd} = p_2 V_o \end{cases} \tag{5}$$

The normalized state space equation of DAB under SPS control can be derived as follows

$$\begin{cases} C\dfrac{du_{C2n}}{dt_n} = p_2 n i_{Ln} - i_{on} \\ L\dfrac{di_{Ln}}{dt_n} = p_1 V_{inn} - p_2 n u_{C2n} \end{cases} \tag{6}$$

Where, $u_{C2n} = u_{C2n}/V_{ref}$, $t_n = tf_n$, $f_n = 1/\left(2\pi\sqrt{LC}\right)$, $Z_o = \sqrt{L/C}$, $i_{Ln} = i_L Z_o/V_{ref}$, $i_{on} = i_o Z_o/V_{ref}$ and $V_{inn} = V_{in}/V_{ref}$. The solution of the inductor current i_L is expressed in Eq.7, where $\omega = 2\pi f_0$.

$$\begin{aligned} i_{Ln} &= \left(i_{Ln}(0) - p_2 i_{on}\right)\cos(\omega t) \\ &+ \left(\frac{1}{2\pi}\frac{di_{Ln}(0)}{dt_n}\right)\sin(\omega t) + p_2 i_{on} \end{aligned} \tag{7}$$

As a result of this, the natural switching surface trajectory for different states can be calculated as follows.

$$\begin{aligned} &\xi_{1,2,3,4} = \left(p_1 V_{inn} - p_2 u_{C2n}\right)^2 - \left(i_{Ln,1,2,3,4} - p_2 i_{on}\right)^2 \\ &-\left(p_1 V_{inn} - p_2\right)^2 + \left(i_{Ln} - p_2 i_{on}\right)^2 \end{aligned} \tag{8}$$

Where, $\xi_{1,2,3,4}$ stands for Mode 1 to 4 respectively. The trajectory for each mode is shown in Fig.4 with color labelled. The red curves depict the steady-state operation under TC, because of the existence of 4 modes, the steady-state of the DAB shows a part of combination of $\xi_{1,2,3,4}$. The variation of

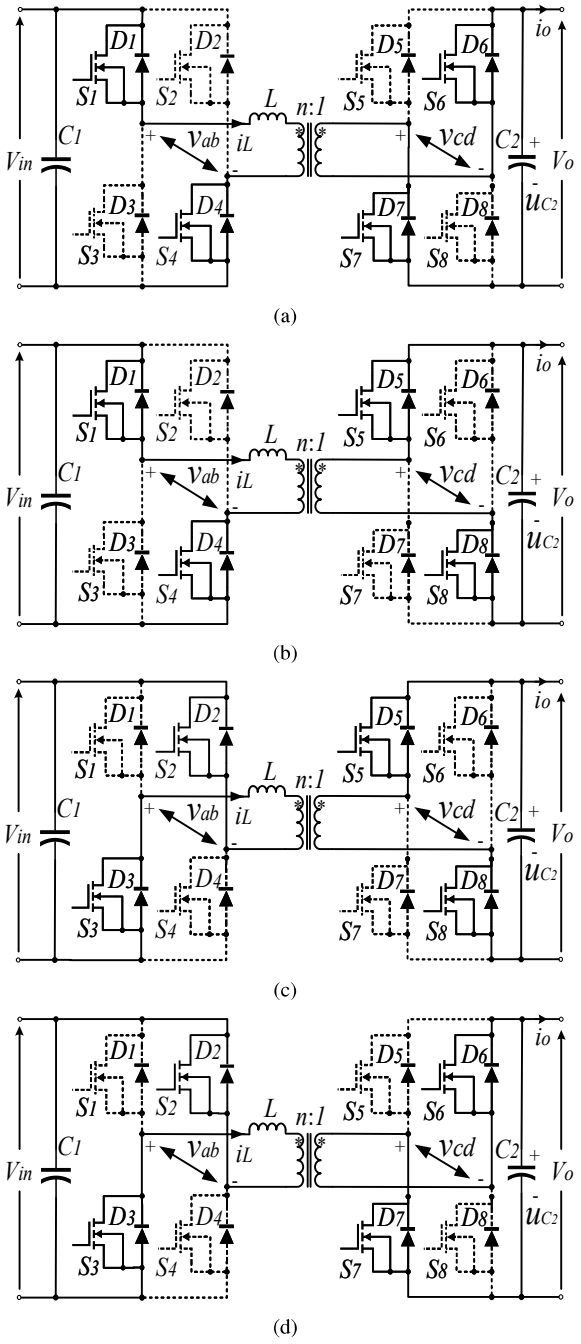

Fig. 3. Switching cases of DAB. (a) Mode 1: $p_1 = 1$,$p_2 = -1$. (b) Mode 2: $p_1 = 1$,$p_2 = 1$. (c) Mode 3: $p_1 = -1$,$p_2 = 1$. (d) Mode 4: $p_1 = -1$,$p_2 = -1$.

this red curve influenced by the output capacitor C_2 and the equivalent load resistance.

As for the CPL, the i_{on} is replaced by $i_{on} = Z_o P/u_{C2n}\Big/V_{ref}^2$ with a constant power. The new trajectory for the CPL is shown in Fig. 5 as the dashed curve and the original NSS is also illustrated. The intersection shows that the NSS can match with CPL trajectory, which is also the key point for final steady-state stabilization. By rebuilding the trajectory of CPL in each mode, there are total four

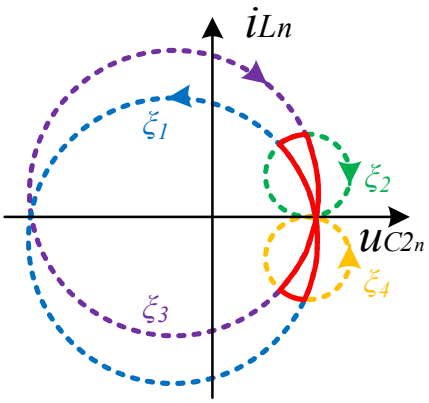

Fig. 4. Natural switching surface based trajectory of DAB under 4 modes control

intersections of the CPL and CRL, at these points, the CPL has the similar characteristic of CRL. Although the trajectories for CRL and CPL are different, the tendency of the CPL trajectory is stable, the output voltage is also operated around V_2 with a small variation, which proved that the NSS based trajectory is possible to work.

III. Simulation Results.

In order to validate the stability of CPL trajectory control, open-loop control, linear controller like closed-loop control with PI controller is chosen for comparison. The simulation parameters are listed as follows, $V_{in} = 80V$, $V_o = 40$, $L = 150\mu$H, transformer turns ratio is $1:1$ and the output capacitance is $C_2 = 200\mu$F.

The simulation results with open-loop are shown in Fig. 6. The step signal stands for load changes, which changes from a 125W CRL to a 300W CPL at 8ms. In open-loop control, the phase-shift ratio is constant with 0.16, which is valid for CRL. However, when changes to CPL, the output voltage decreases to 0 rapidly, which is labeled as red color. The system is unstable. The reason can be summarized as follows. If there is a disturbance which causes a reduction of the current, at the new current point, the previous output voltage is less than the load voltage, thus, the current decreases further and make the operating status point moves away of the stable point. Which means the open-loop control with a fixed phase-shift ratio is not possible to control the CPL.

Compared with open-loop control, simulation results under closed-loop control with PI controller are shown in Fig. 7. Under closed-loop control, the start-up stage is faster than open-loop control because the phase-shift ratio is 0.5 with 1 per-unit transmission power. After 1ms, the phase-shift ratio varies around 0.16. The load changes from a 125W CRL to a 300W CPL at 4ms. In closed-loop control, the phase-shift ratio varies with the output of PI controller, which is stable under CRL. However, when changes to CPL, the output voltage decreases to 0 gradually as labeled in red color. The system is unstable finally. Additionally, the PI controller is effective in a limited range, varies PI parameters may result in different final states, which leads to a difficult prediction of the CPL.

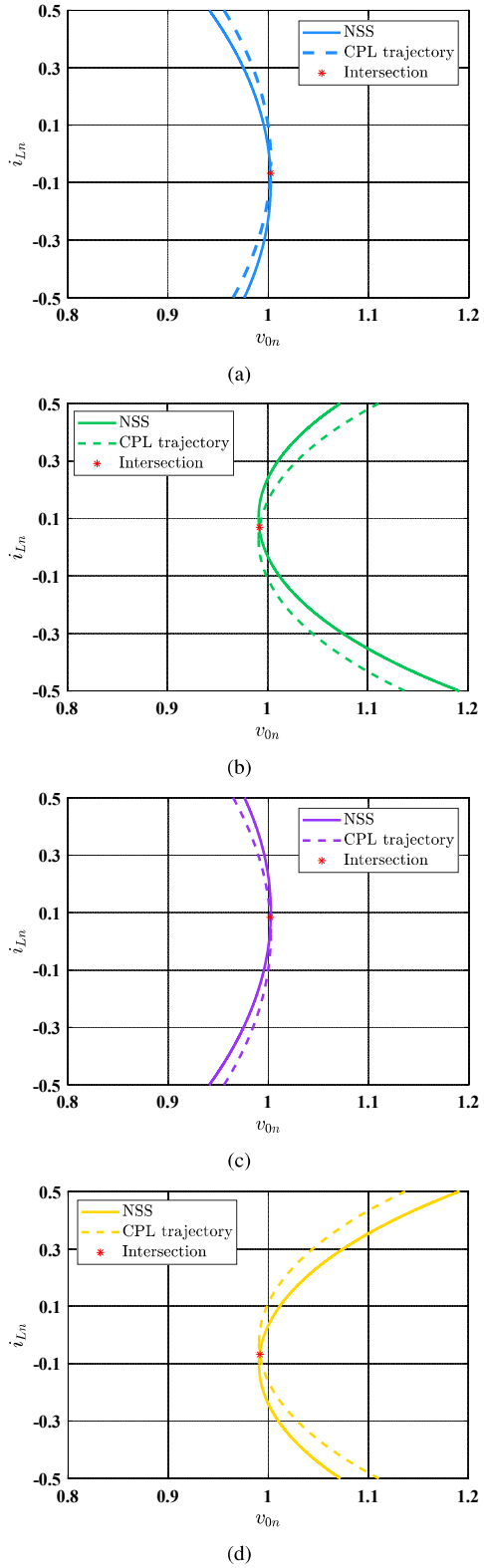

Fig. 5. NSS and CPL trajectory under different modes of DAB. (a) Mode 1: $p_1 = 1$,$p_2 = -1$. (b) Mode 2: $p_1 = 1$,$p_2 = 1$. (c) Mode 3: $p_1 = -1$,$p_2 = 1$. (d) Mode 4: $p_1 = -1$,$p_2 = -1$.

The simulation results with TC are shown in Fig. 8, which shows the main merit in start-up stage. It merely takes 0.3ms to

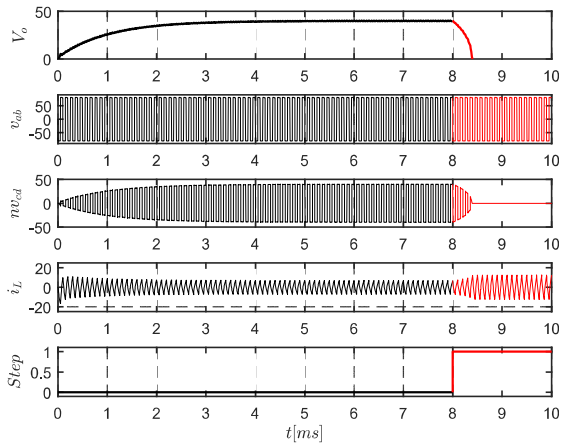

(a)

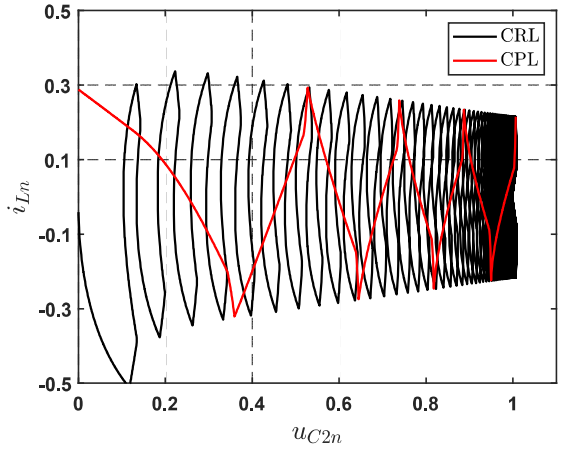

(b)

Fig. 6. Simulation results of DAB converter at start-up stage and switch load from CR to CP under PI controller. (a) Waveforms of output voltage V_o, primary bridge voltage v_{ab}, secondary bridge voltage v_{cd}, inductor current i_L and step. (b) Phase plane of i_{Ln} with respect to u_{C2n}.

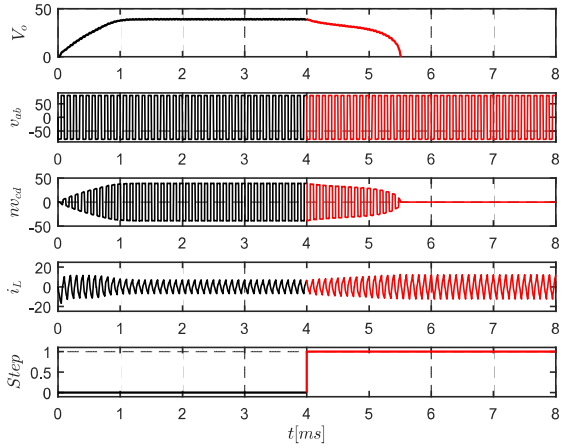

(a)

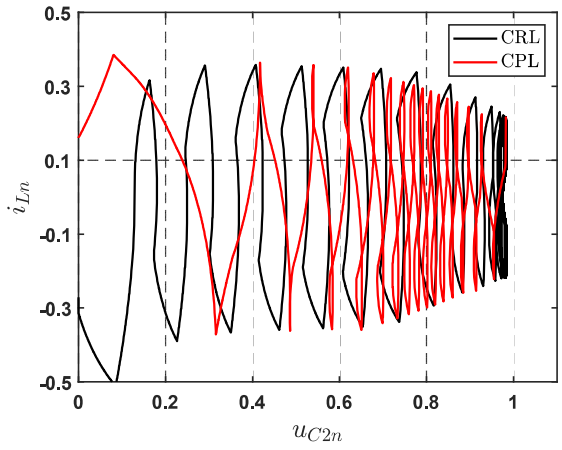

(b)

Fig. 7. Simulation results of DAB converter at start-up stage and switch load from CR to CP under PI controller. (a) Waveforms of output voltage V_o, primary bridge voltage v_{ab}, secondary bridge voltage v_{cd}, inductor current i_L and step. (b) Phase plane of i_{Ln} with respect to u_{C2n}.

finish the start-up stage, the fast dynamic response is validated. Because in TC, the frequency is not constant, which is the main difference compared with traditional control methods. The Load changes from a 125W CRL to a 300W CPL at 1ms. The transient-state is shrunk into one switching cycle and the output voltage is stable as expected. Compared with the open loop control and the closed-loop control with PI controller. The start-up stage and the transient-state in the dynamic response are improved effectively.

IV. Conclusion

This paper analysed the trajectory control based on natural switching surface, especially for constant power load application. By rebuilding the state-space equation with a fixed power load, the trajectory for CPL is obtained. Under the trajectory control, the DAB shows the fast start-up stage. Additionally, the transient-state from CRL to CPL is also reduced to less than one switching cycle, the stability of CPL is validated effectively.

V. Acknowledgement

This work was supported by the Research development fund of XJTLU (RDF-16-01-10, RDF-17-01-28), the Research Enhancement fund of XJTLU (REF-17-01-02), the Suzhou Prospective Application programme (SYG201723), and the XJTLU Key Programme Special Fund (KSF-A-08, KSF-E-13KSF-T-04).

References

[1] O. Cornea, G. Andreescu, N. Muntean, and D. Hulea, "Bidirectional power flow control in a dc microgrid through a switched-capacitor cell hybrid dcdc converter," *IEEE Trans. Ind. Electron.*, vol. 64, no. 4, pp. 3012–3022, April 2017.

[2] Huiqing Wen, Kai Zheng, and Yang Du, "Hierarchical coordinated control for dc microgrid with crowbar and load shedding control," in *2017 IEEE 3rd International Future Energy Electronics Conference and ECCE Asia (IFEEC 2017 - ECCE Asia)*, June 2017, pp. 2208–2212.

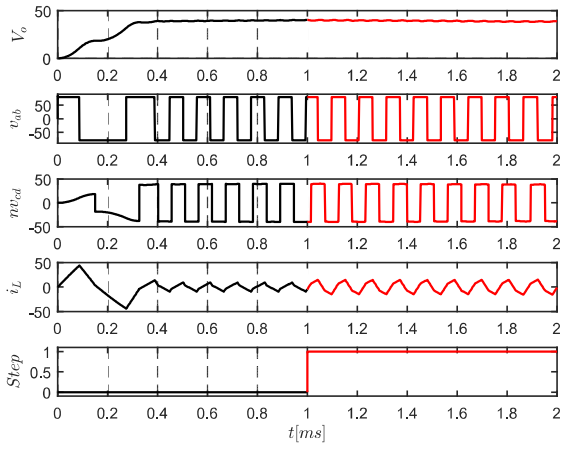

(a)

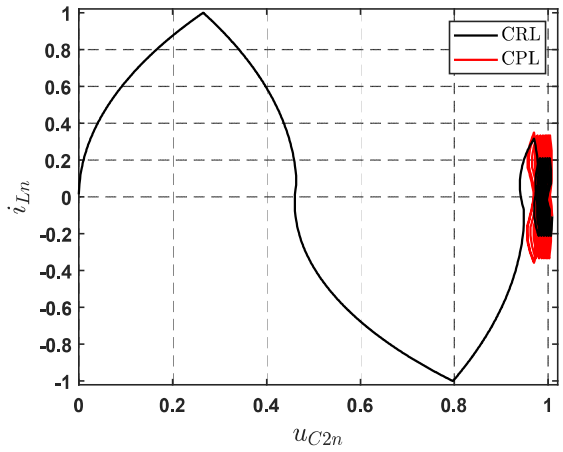

(b)

Fig. 8. Simulation results of DAB converter at start-up stage and switch load from CR to CP under ITC. (a) Waveforms of output voltage V_o, primary bridge voltage v_{ab}, secondary bridge voltage v_{cd}, inductor current i_L and step. (b) Phase plane of i_{Ln} with respect to u_{C2n}.

[3] Huiqing Wen and Runze Yang, "Power management of solid state transformer in microgrids," in *2016 IEEE PES Asia-Pacific Power and Energy Engineering Conference (APPEEC)*, Oct 2016, pp. 1399–1404.

[4] H. Wen and Weiqiang Zhu, "Control and protection of dc microgird with battery energy storage system," in *2016 IEEE International Conference on Power Electronics, Drives and Energy Systems (PEDES)*, Dec 2016, pp. 1–6.

[5] H. Wen, B. Su, and W. Xiao, "Design and performance evaluation of a bidirectional isolated dc-dc converter with extended dual-phaseshift scheme," *IET Power Electronics*, vol. 6, no. 5, pp. 914–924, May 2013.

[6] B. Su, H. Wen, J. Zhang, and Z. Lu, "A soft-switching post-regulator for multi-outputs dual forward dc/dc converter with tight output voltage regulation," *IET Power Electronics*, vol. 6, no. 6, pp. 1069–1077, July 2013.

[7] G. Chen, Y. Deng, K. Wang, Y. Hu, L. Jiang, H. Wen, and X. He, "Topology derivation and analysis of integrated multiple output isolated dcdc converters with stacked configuration for low-cost applications," *IEEE Transactions on Circuits and Systems I: Regular Papers*, vol. 64, no. 8, pp. 2207–2218, Aug 2017.

[8] J. Yang, D. Yu, H. Cheng, X. Zan, and H. Wen, "Dual-coupled inductors-based high step-up dc/dc converter without input electrolytic capacitor for pv application," *IET Power Electronics*, vol. 10, no. 6, pp. 646–656, 2017.

[9] Y. Wang, X. Chen, H. Tang, Y. Yang, H. Wen, and Y. Lin, "Design a modified bi-directional converter for solar led lighting system," in *2018 IEEE Energy Conversion Congress and Exposition (ECCE)*, Sep. 2018, pp. 4733–4737.

[10] H. Shi, H. Wen, Y. Hu, Y. Yang, and Y. Wang, "Efficiency optimization of dc solid-state transformer for photovoltaic power systems," *IEEE Trans. Ind. Electron.*, pp. 1–1, 2019.

[11] Q. Bu, H. Wen, J. Wen, Y. Hu, and Y. Du, "Transient dc bias elimination of dual active bridge dc-dc converter with improved triple-phase-shift control," *IEEE Trans. Ind. Electron.*, pp. 1–1, 2019.

[12] H. Shi, H. Wen, Y. Hu, and L. Jiang, "Reactive power minimization in bidirectional dcdc converters using a unified-phasor-based particle swarm optimization," *IEEE Trans. Power Electron.*, vol. 33, no. 12, pp. 10 990–11 006, Dec 2018.

[13] H. Shi, H. Wen, and Y. Hu, "Deadband effect and accurate zvs boundaries of gan-based dual active bridge converters with multiple-phase-shift control," *IEEE Trans. Power Electron.*, pp. 1–1, 2020.

[14] A. Emadi, A. Khaligh, C. H. Rivetta, and G. A. Williamson, "Constant power loads and negative impedance instability in automotive systems: definition, modeling, stability, and control of power electronic converters and motor drives," *IEEE Trans. Veh. Technol.*, vol. 55, no. 4, pp. 1112–1125, July 2006.

[15] X. Zhang, D. M. Vilathgamuwa, K. Tseng, B. S. Bhangu, and C. J. Gajanayake, "Power buffer with model predictive control for stability of vehicular power systems with constant power loads," *IEEE Trans. Power Electron.*, vol. 28, no. 12, pp. 5804–5812, Dec 2013.

[16] M. K. Zadeh, R. Gavagsaz-Ghoachani, J. Martin, B. Nahid-Mobarakeh, S. Pierfederici, and M. Molinas, "Discrete-time modeling, stability analysis, and active stabilization of dc distribution systems with multiple constant power loads," *IEEE Trans. Ind. Appl.*, vol. 52, no. 6, pp. 4888–4898, Nov 2016.

[17] A. M. Rahimi and A. Emadi, "An analytical investigation of dc/dc power electronic converters with constant power loads in vehicular power systems," *IEEE Trans. Veh. Technol.*, vol. 58, no. 6, pp. 2689–2702, July 2009.

[18] M. Anun, M. Ordonez, I. G. Zurbriggen, and G. G. Oggier, "Circular switching surface technique: High-performance constant power load stabilization for electric vehicle systems," *IEEE Trans. Power Electron.*, vol. 30, no. 8, pp. 4560–4572, Aug 2015.

[19] H. Shi, H. Wen, and Z. Cao, "Optimal minimized reactive power boundary control based on the six natural switch-

ing surface," in *2018 IEEE International Conference on Power Electronics, Drives and Energy Systems (PEDES)*, Dec 2018, pp. 1–6.

[20] H. Wen and Y. Gajadur, "Improved natural switching surface control for the bidirectional dual active bridge converter," in *2018 IEEE International Conference on Power Electronics, Drives and Energy Systems (PEDES)*, Dec 2018, pp. 1–6.

[21] G. G. Oggier, M. Ordonez, J. M. Galvez, and F. Luchino, "Fast transient boundary control and steady-state operation of the dual active bridge converter using the natural switching surface," *IEEE Trans. Power Electron.*, vol. 29, no. 2, pp. 946–957, Feb 2014.

[22] G. G. Oggier and M. Ordonez, "Boundary control of full-bridge zvs: Natural switching surface for transient and steady-state operation," *IEEE Transactions on Industrial Electronics*, vol. 61, no. 2, pp. 969–979, Feb 2014.

[23] ——, "High-efficiency dab converter using switching sequences and burst mode," *IEEE Transactions on Power Electronics*, vol. 31, no. 3, pp. 2069–2082, March 2016.